Journal of Statistical Physics, Vol. 54, Nos. 5/6, 1989

Structure Changes Induced by External Multiplicative Noise in the Electrohydrodynamic Instability of Nematic Liquid Crystals

Shoichi Kai,[1] Hidehiko Fukunaga,[1] and Helmut R. Brand[2]

Received March 30, 1988; September 20, 1988

We study the influence of external multiplicative noise on the electrohydrodynamic instability (EHD) in nematic liquid crystals. It turns out that the correlation time τ_N and the intensity Q of the noise are the crucial parameters to control the system. Different types of noise lead to minor quantitative changes when compared to Gaussian white noise, leaving the qualitative aspects unchanged. With increasing noise intensity the threshold for the onset of the first instability changes drastically. We observe that the curvature arising when the threshold of the various instabilities is plotted as a function of the noise intensity changes as one is going, e.g., from the onset of Williams domains (WD) to the onset of the grid pattern (GP). This result reflects the transition in the flow structure from two-dimensional (WD) to three-dimensional (GP, DSM) flow patterns. As the intensity of the noise is increased further, the onset of the first instability becomes more complex. The measurement of the nonlinear onset time shows a strong dependence on the noise intensity Q, which is linear for WD and GP well above onset. The linear onset time shows an unexpected dependence on the noise intensity close to the onset of the first instability. For sufficiently long correlation times of the noise, a destabilization by noise is obtained.

KEY WORDS: Spatial structures; multiplicative noise; electrohydrodynamics; stabilization; destabilization; instability; pattern formation; colored noise; additive noise.

1. INTRODUCTION

Stochastic processes can be classified into two types. The most common processes are associated with an additive random force. The other class is

[1] Department of Electrical Engineering, Kyushu Institute of Technology, Tobata, Kitakyushu, 804, Japan.

[2] FB 7, Physik, Universitaet Essen, D 43 Essen 1, West Germany.

0022-4715/89/0300-1133$06.00/0

made up of stochastic processes containing a coupling between the stochastic variable and the random force. The former class has already been investigated in detail and is well understood. The latter type frequently are called multiplicative stochastic processes (MSP) and are not as well understood; a number of unsolved problems exist in the nonlinear domain. MSP have been investigated in various fields recently, such as in optical systems and lasers,[1–14] in the magnetic Fredericksz transition of nematic liquid crystals,[15–19] in electrical circuits,[20–22] and in the electrohydrodynamics (EHD) of liquid crystals.[23–29] In EHD an MSP is realized when one applies externally an electric noise field together with the sinusoidal deterministic field to a thin layer of a nematic liquid crystal; this setup has been considered in refs. 23–29.

For MSPs most theoretical studies and analog simulations concentrate on spatially uniform systems described by an equation of the form $\dot{u} = f(u) + g(u)\,\xi$,[1–22,29–39] where ξ is typically Gaussian white noise. A broad variety of results emerges. The number of peaks of the stationary probability distribution can change as a function of the noise intensity; the relaxation rates of such a system can depend strongly on the noise intensity and the threshold value for the onset of an instability can be enhanced, i.e., externally applied noise (of multiplicative type) can induce the stabilization of a system. Detailed theoretical studies for the magnetic Fredericksz transition under the influence of an additional fluctuating magnetic field in nematic liquid crystals have been reported recently.[15–19] According to these studies, the threshold field H_C for the onset of the Fredericksz transition increases with an increase of the strength of the external fluctuating magnetic field and with a decrease in the correlation time of the noise field.[15]

These theoretical studies address one-variable systems without any spatial structure. The phenomena observed experimentally in spatially extended systems, however, should be discussed including spatial degrees of freedom[40] and one needs to address the question of how multiplicative noise influences a spatial structure and its kinetics. Previous theories for MSP in EHD did not examine the spatial patterns explicitly and mainly concentrated on the explanation of the experimentally observed threshold shift for the onset of the first spatial structure. The influence of spatial variations on MSP is thus not well understood.

In the present paper we report that for MSP in EHD transitions between different spatial structures are induced by the superposition of noise on a sinusoidal electric field and that the occurrence of these transitions depends systematically on the correlation time and the intensity of the noise (in ref. 41 we briefly indicated some of the results). In Section 2 we describe the experimental setup, including the various types of applied

noise and the procedure used to evaluate the dynamic properties from the dynamic birefringence. In Section 3 the experimental results for MSP are described and discussed. Section 4 contains a summary and the conclusions emerging from the present study.

2. EXPERIMENT

2.1. Sample Preparation

The compound used in the present study is the material MBBA [*N*-(*p*-methoxybenzylidene)-*p*-butylaniline], which shows a nematic phase at room temperature. This compound is sandwiched between two horizontal glass plates coated with SnO_2 conducting electrodes.[42–45] The thickness d of the sandwiched cells used here ranges from 100 to 110 μm. The lateral dimensions are typically 100 times the thickness. The plates are rubbed to obtain homogeneous alignment. The threshold voltage V_C for Williams domains (WD) ($f < f_C$) lies between 6 and 10 V, and V_C for the oscillatory instability of the director ($f > f_C$) is between 40 and 300 V as a function of applied frequency. Here f and f_C are the frequency of the applied field and the critical frequency separating two regimes, the conducting ($f < f_C$) and the dielectric ($f > f_C$) regime.[42–46] We paid special attention to aging effects of the sample. We waited, for example, until changes of V_C and f_C as a function of time became very small and then we used the sample. During one experiment (with a typical duration of 2 weeks) the changes of V_C and f_C were less than 2%. We also used different samples for different experiments. Although we used a total of five different samples throughout the present study, we discuss here mainly the results for d close to 100 μm. The quantitative values measured depend on the sample but the qualitative behavior does not change. V_C was determined from the sharp decrease of the transmitted intensity of the light due to the onset of the spatial structure. For this measurement of the threshold, we used a photodiode as a light source and a phototransistor as a detector. The information thus obtained is for a large area of about 3×3 mm^2 in the present measurement of the threshold. The temperature during the experiments is controlled up to ± 0.05 deg using a copper container with a double wall.

2.2. Types of Externally Applied Noise

Different types of noise are applied to the sample, which are realized by using a commercially available noise generator (NF Co. WG722), which produces a quasirandom noise with a period $T_p \approx 510$ days for a 20-μsec clock.

The interval distribution between two binary pulses can be described by a Poissonian distribution (Fig. 1),

$$N(n, \nu) = \frac{\nu^n}{n!} \exp(-\nu) \tag{1}$$

where n is the unit time delay given by $\Delta t/b$, where Δt is the time interval between two successive pulses, and b is the minimum width of the binary pulse, which depends on the clock frequency of the shift register, for example, $b = 20$ μsec for a 20 μsec clock and 200 μsec for a 200-μsec clock. Since pulses are not generated by superposition, one cannot observe a pulse during a time lag Δt shorter than twice the pulse width $2b$.

In Fig. 1 we see that a Gaussian distribution

$$N(\Delta t) = (2\pi)^{-1/2} \sigma_t^{-1} \exp\left(-\frac{(\Delta t - 2b)^2}{2\sigma_t^2} \right) \tag{2}$$

also fits quite well with parameters $2b = 40$ μsec and $\sigma_t = 50$ μsec, as shown by the dotted line.

The experimentally observed power spectrum $P(\omega)$ agrees well with a Gaussian white noise spectrum up to $f = 20$ kHz (Fig. 2). Other types of noise are produced from this binary noise by filtering with a special elec-

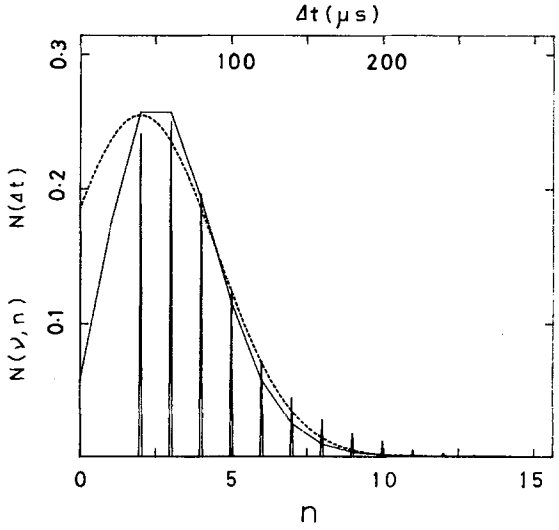

Fig. 1. Generation probability density of the noise pulses for the 20 μsec clock used in the present study. The Gaussian distribution given in Eq. (2) is plotted as a dashed line.

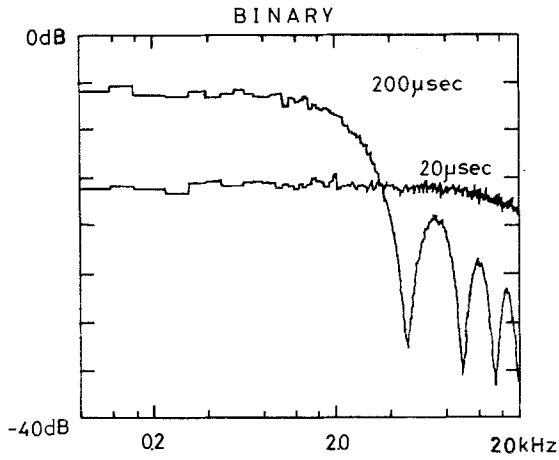

Fig. 2. Power spectrum of a binary pulse.

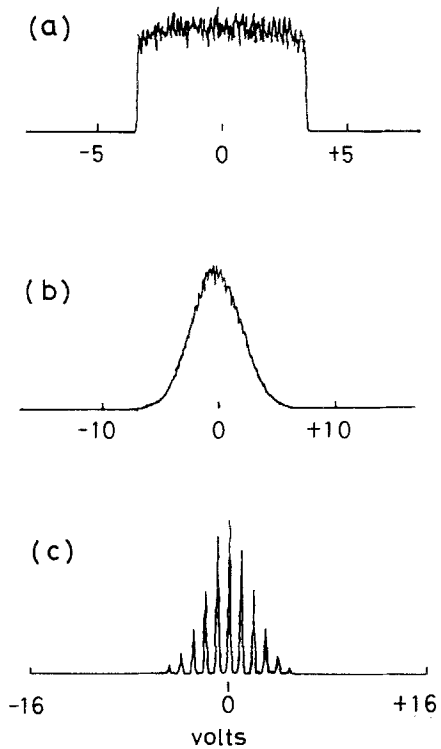

Fig. 3. Probability density of the amplitudes for various types of noise. (a) Uniform ($V_N = 2.65$ V), (b) Gaussian ($V_N = 2.65$ V), (c) binomial ($V_N = 2.88$ V).

trical technique. Figure 3 shows the probability density functions of the wave amplitudes used here. The intensity of the noise is determined by $Q = V_N^2 = \langle V(0)^2 \rangle$ using a fast Fourier transform (FFT) analyzer (Iwatsu Co. SM-2100A). The correlation time of the noise is determined by taking the autocorrelation function or the bandwidth of the power spectrum using this analyzer. For the study of MSP, this external noise is superposed on the deterministic sinusoidal field and then applied to a liquid crystal sample.

2.3. Measurement of the Temporal Evolution of the Director Angle Using Birefringence

The method used is basically the same as the one used for the measurement of the evolution of the director angle in the Fredericksz transition of nematic liquid crystals.[47] We evaluate the linear time constant, $\exp(\pm t/\tau_L)$, using this type of dynamical birefringence technique. The director is initially aligned homogeneously at $\Theta = 0$. Then we assume the following linear temporal evolution of the director:

$$\frac{d\Phi}{d\Theta} = \frac{d\Theta}{dt} = \tau_L^{-1}(\varepsilon)\,\Theta \tag{3}$$

when an electric field larger than the theshold ($V > V_C$) is applied. Here $\varepsilon = (V^2 - V_C^2)/V_C^2$ and Φ is a potential. The precise expression for the coefficient τ_L^{-1} is complicated and depends on the elastic, dielectric, and viscous coefficients of the nematic liquid crystal.[48] When the external voltage is varied from $V_0 < V_C$ to $V_A > V_C$, the system falls into the most stable state of the potential curve Φ_A in Fig. 4, where V_0 is a certain bias voltage lower than V_C, used to obtain alignment parallel to the glass plates, and where V_A is higher than V_C.

Since a liquid crystal shows birefringence, the phase difference ϕ between the ordinary and the extraordinary light beams passing through the sample gradually changes with the temporal change of the director angle according to the equation[47]

$$\phi(t) = \left(\frac{\pi d}{\kappa}\right) \Theta^2(t)(n_e - n_o) \tag{4}$$

where κ, n_e, and n_o are the wavelength of the light and the refractive indices for an extraordinary and an ordinary light beam, respectively. Thus, the oscillation of the light intensity can be observed for each 2π period of $\phi(t)$, following the temporal evolution of $\Theta(t)$. The experimental setup and

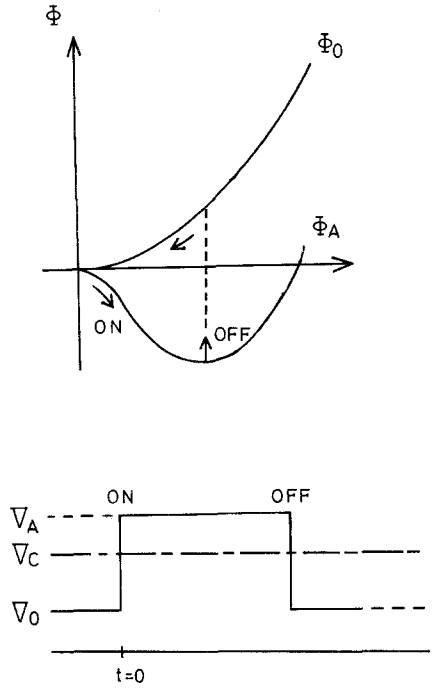

Fig. 4. Potential profile above threshold V_C and below threshold V_C.

the oscillatory signal detected are shown in Fig. 5. Here N shows the Nth oscillation. The inverse of the interval is proportional to the slope of Φ. The time constant is obtained from the interval of these oscillations as follows:

$$\tau_L = \frac{t_{N+1} - t_N}{\ln[(N+1)/N]} \tag{5}$$

according to Eq. (3). This holds only for small N and we always choose here $N = 1$. Qualitatively we can infer from the signal shown in Fig. 5 that the slope of Φ is very flat for the initial stage and for the steady state, but steep for the transient region (i.e., for the short interval of the signal shown in Fig. 5).

In the same manner, we also measured the relaxation time, switching the field from V_A to V_0. The divergent tendencies as V_C is approached from both sides are clearly observed (Fig. 6). This dependence on ε can be described by Eq. (3) in which τ_L is proportional to ε^{-1}. Another important time constant to describe the dynamics of the growth is the nonlinear

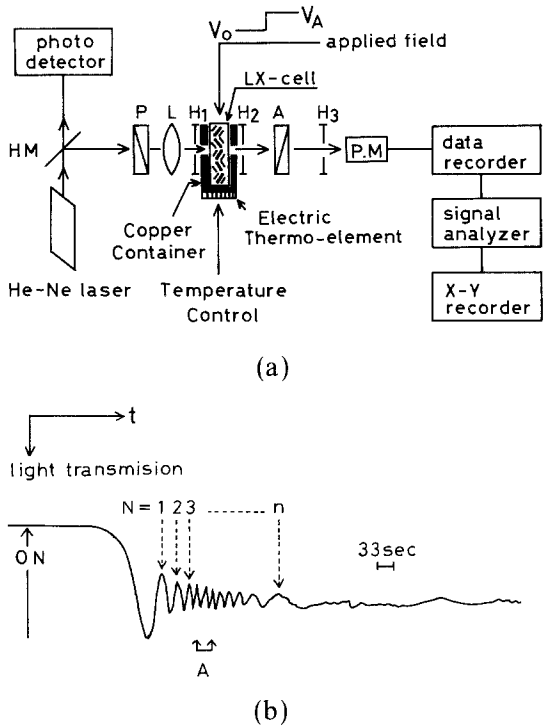

Fig. 5. (a) Experimental setup and (b) an example of the detected signal. A: analyzer; H_1, H_2, H_3: pin holes; HM: half-mirror; L: lens; P: polarizer.

growth time, for which we chose the time τ_r in which 90% of the final amplitude is reached and which contains the influence of the nonlinear effects not contained in Eq. (3).[26,28,29]

3. RESULTS AND DISCUSSION

3.1. Convective Patterns in EHD

When the field reaches V_C, one finds first a roll pattern called Williams domains (WD) (Fig. 7a). As the voltage is increased, these rolls start to fluctuate in time with a characterictic ε-dependence (fluctuating Williams domains, FWD) and eventually a transition to the grid pattern (GP) at V_{GP} (typically at 1.5–2.0 times V_C) takes place (Fig. 7b). As the applied voltage is stepped up further, the spatially and temporally

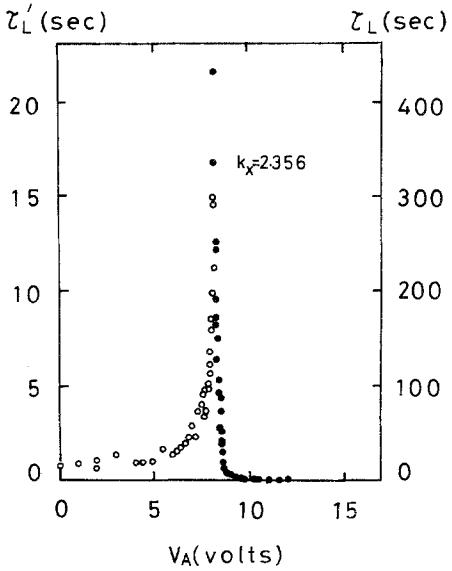

Fig. 6. Linear relaxation time $\tau_L(V < V_C)$ and growth time $\tau_L(V > V_C)$ as a function of applied voltage for sample 1: $d = 100\ \mu$m, aspect ratio (ratio of lateral dimension to cell thickness) 100.

incoherent regime, usually called the dynamic scattering mode (DSM), is formed (Fig. 7c). Thus, many interesting dissipative structures have been observed in the EHD of nematic liquid crystals.[43–46,49]

3.2. Effects of Multiplicative External Noise

3.2.1. Threshold Shifts for the Onset of Instabilities Induced by the Application of Various Types of External Noise. In Fig. 8 ($d = 100\ \mu$m, sample 3), typical results of the threshold shift for the first instability are plotted as a function of the strength of the noise V_N ($= Q^{1/2}$). Here we used two types of noise distinguished by the probability density distribution of the amplitude, namely uniform and binomial noise. The frequency of the deterministic field is 30 Hz and the correlation times are 65 and 5 μsec for both types of noise. As seen in Fig. 8, no dependence of the threshold shift on the amplitude distribution of the noise can be observed as long as τ_N is the same. We also stress that there is no dependence on the frequency of the deterministic field f for $f < 50$ Hz. Here we note a change in curvature of $V_C(V_N)$ at $V_N^* \approx 17$ V. Theoretical studies predict a linear relation between the threshold shift and the amplitude of the noise,[33,35] but the slope of the experimental curve changes as a function of the noise strength.

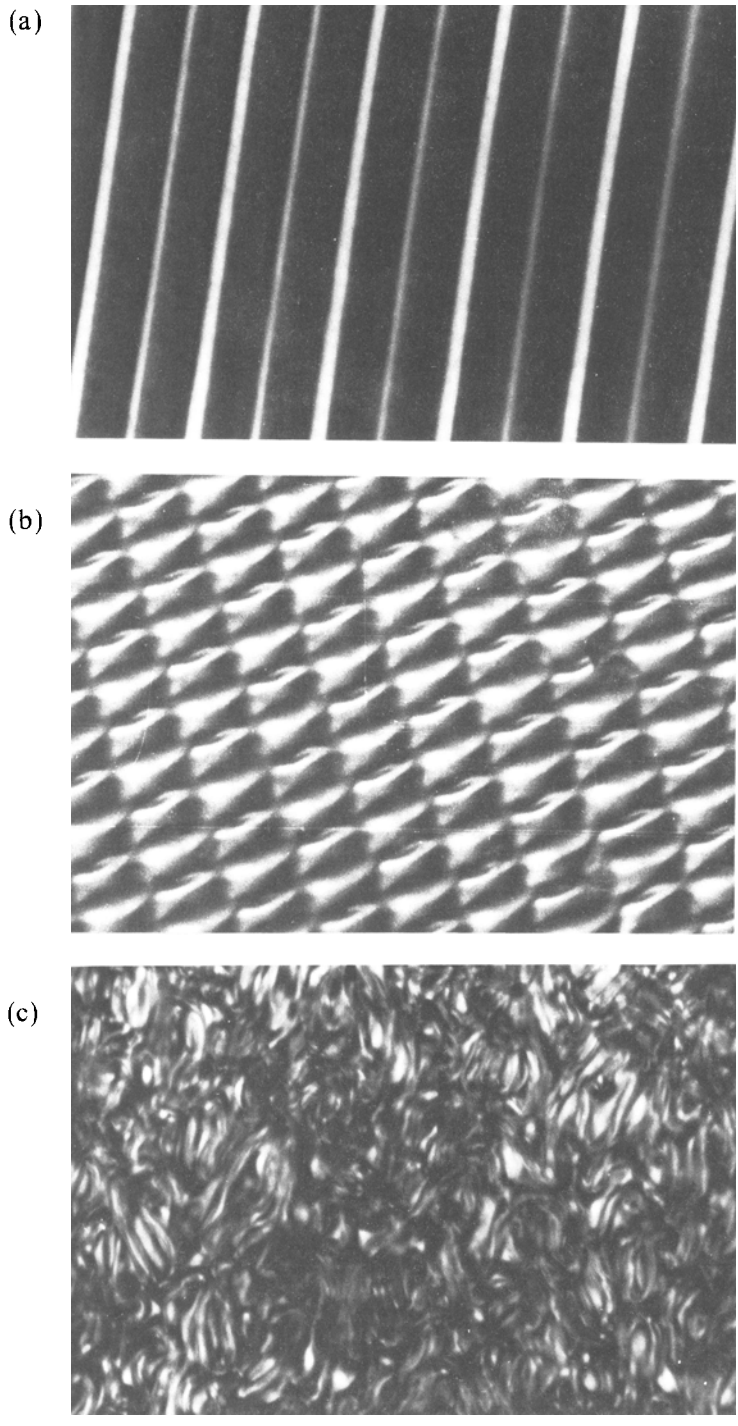

Fig. 7. Typical convective patterns observed in the conductive regime ($f < f_C$) for sample 2: $d = 100$ μm, aspect ratio 50. (a) Williams domains (two-dimensional convective flow), (b) grid pattern (three-dimensional cellular convective flow),[43,44] (c) dynamic scattering mode (turbulent flow).

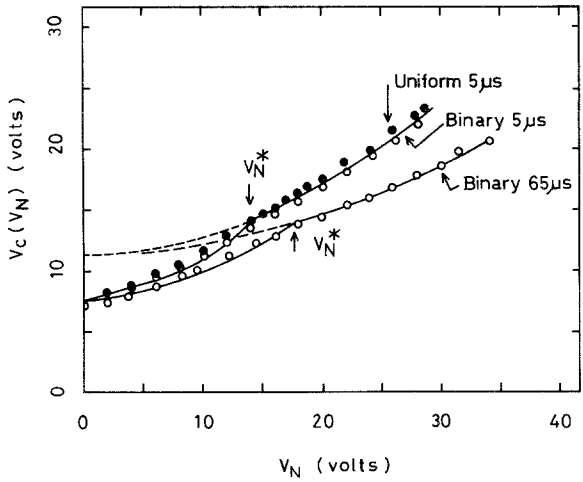

Fig. 8. Phase diagram for two types of noise with different probability densities (binary and uniform) for sample 3: $d = 100\ \mu$m, aspect ratio 40, $f_C = 360$ Hz.

In particular, we cannot draw a straight line for $\tau_N > \tau_N^*$, as seen in Fig. 9 (the definition of τ_N^* is shown in Fig. 10). Therefore we fit our data to the equation

$$V_C(V_N) = \beta_2 V_N^2 + \beta_1 V_N + \beta_0 \tag{6}$$

for both curves for $V_N < V_N^*$ and $V_N > V_N^*$, respectively, where β_0, β_1, and

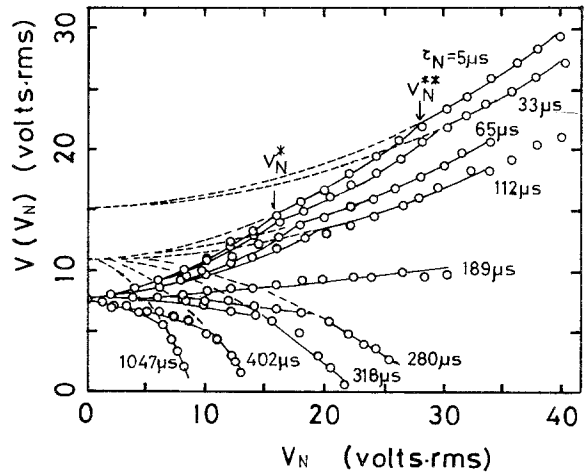

Fig. 9. Dependence of the phase diagram on the correlation time τ_N. Note that the extrapolations converge into the threshold voltage for the onset of each instability (WD, GP, and DSM) even for negative slopes (sample 3). V_N^* and V_N^{**} are marked for $\tau_N = 5\ \mu$sec.

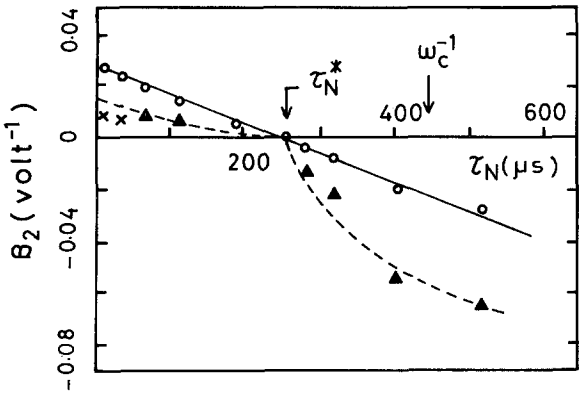

Fig. 10. The coefficient β_2 in Eq. (6) plotted as a function of τ_N. At $\tau_N^* \sim 255$ sec, the coefficient changes from positive to negative values (sample 3). (○) $V_N < V_N^*$, (▲) $V_N^* < V_N < V_N^{**}$, (×) $V_N^{**} < V$.

β_2 are coefficients obtained from the experimental results by the last-mean-square method. A higher noise intensity always leads to a stabilization of the periodic structure for $\tau_N \ll \tau_C$. These shifts can be intuitively explained qualitatively by taking into account that the external noise reduces the amount of space charge by inducing a random oscillation of the director of NLC, which must be stored to cause convection by the Carr–Helfrich mechanism.[42]

The correlation time of the noise strongly influences the structure of the phase diagram. Figure 9 shows the dependence of the phase diagram on the correlation time τ_N of the externally applied noise. The measurements for various τ_N in Figs. 8 and 9 were done in the random sequence $\tau_N = 5$, 65, 33, 318, 1047, 112, 189, 280, and 402 μsec to rule out completely the possibility that aging of the sample plays any role. As τ_N becomes shorter, the slope of the noise dependence in the phase diagram becomes steeper. On the other hand, as τ_N approaches the characteristic time $\tau_C = \omega_C^{-1}$ of the deterministically applied field, corresponding to 442 μsec ($f_C = 360$ Hz), the condition $\tau_N \ll \tau_C$ no longer holds and the slope becomes flatter. Increasing τ_N further, we observe that the threshold shift happens toward the negative direction, i.e., a destabilization by noise results.

When each curve between changes of curvature is fitted to Eq. (6), a systematic change of the coefficient β_2, which characterizes the curvature, can be observed (Fig. 9). The crossover correlation time τ_N^* of the noise is obtained to be 255 μsec in this cell ($d = 100$ μm, $\Gamma = 40$), which is identical to 60% of the value of τ_C (~ 442 μsec) for the oscillatory instability of EHD. For $\tau^*_N < \tau_N$ the noise works in a cooperative fashion with the deterministic field. Accordingly, the external noise can destabilize the system in this case.

We would like to stress the following results. The noise intensities for which a change in curvature occurs depend on τ_N; they are shifted to higher noise intensity for decreasing τ_N, which also leads to an increase in the slope. Extrapolations of respective parts of the curves for $V_N < V_N^*$, $V_N^* < V_N < V_N^{**}$, and $V_N^{**} < V_N$ give three characteristic voltages $V_C(0) = 7.6$ V, $V_{C1}(0)$ $[\sim 1.5\, V_C(0)]$, and $V_{C2}(0)$ $[\sim 1.97\, V_C(0)]$ for the intersection at $V_N = 0$, which respectively correspond to the thresholds of WD, of FWD, and of GP in the absence of the external noise. We note that we can observe DSM at threshold when V_N is further increased. Here DSM represents the first strongly irregular pattern (although there are three types of DSM distinguished in the literature[44,45]). From these observations it can be concluded that for $V_N > V_N^{**}$, WD is unstable, whereas the GP is stable as the first pattern at the onset point (Fig. 9). That is, an exchange of the occurring stable spatial structure is induced by noise. Visual observations for these three regions appearing between changes in curvature are the following. For $V_N < V_N^*$, steady WD are observed for the entire region of the cell. For $V_N^{**} < V_N < V_N^{***}$, the GP is commonly formed after fluctuations of rolls for a long but transient period of time, and for $V_N > V_N^{***}$ an irregular pattern, DSM, aperiodic in time and in space results. Here V_N^{***} is the threshold for the direct transition to DSM.[26] Between V_N^* and V_N^{**}, WD fluctuate irregularly with a characteristic distance of about four to eight rolls.

All slopes, even for various τ_N, converge into three characteristic voltages with different slopes for vanishing noise. The same happens for $\tau_N > \tau_N^*$, that is, at least two changes in curvature have been observed and they converge into the respective characteristic voltages although those slopes are negative. This clearly demonstrates that noise influences different spatial patterns in different ways (Fig. 9). Such a dependence of the coefficient β_2 is also apparent from Fig. 10. When there is a wide range of observation for V_N, a number of changes in curvature corresponding to a number of successive transitions to fully developed turbulence are observed.[43–45]

Figure 11 shows the correlation time dependence of the threshold V_C of a deterministic field for fixed V_N. For constant V_N, V_C increases with decreasing τ_N (Fig. 11a). The relation between V_C and τ_N^{-1} for fixed V_N is roughly given by $V_C \sim (\tau_N^0 - \tau_N)^{-1/2}$. For a certain value of τ_N $(= \tau_N^0)$, V_C becomes zero, which corresponds to the onset of convection without a deterministic field. In other words, the instability can also be induced by noise only without any deterministic field (i.e., $V_C = 0$), depending on the correlation time τ_N and the amplitude V_N of the noise. From our experiments we can summarize our results in the empirical equation

$$V_N^0 \approx 6.5 \exp(A/\tau_N) \quad \text{(volts)} \tag{7}$$

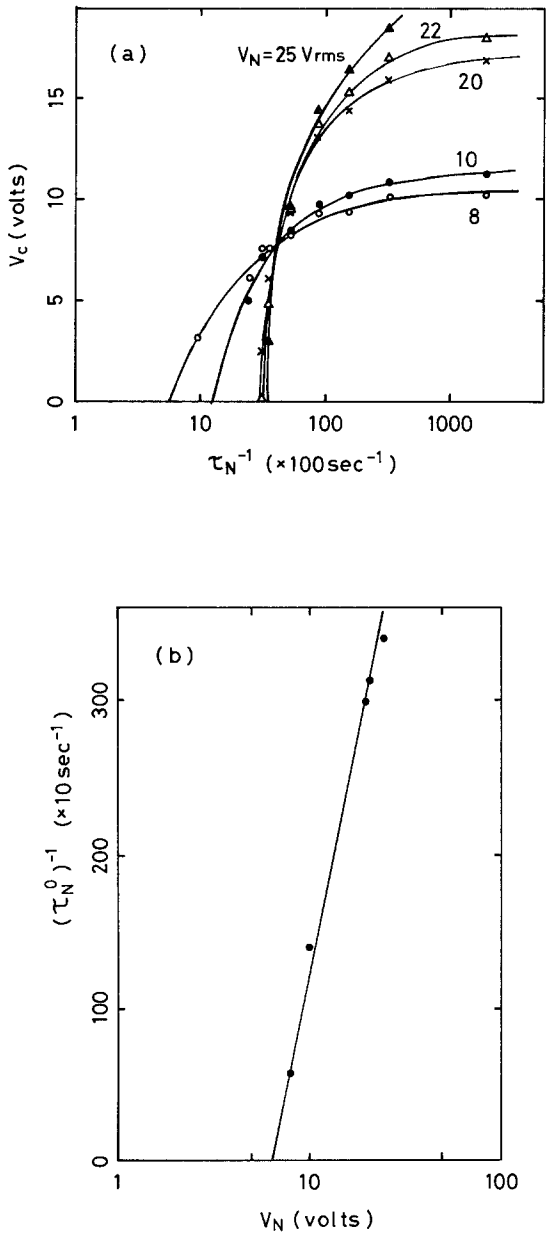

Fig. 11. Threshold voltage V_C as a function of the correlation time τ_N of the noise for (a) fixed noise amplitude V_N and (b) V_N as a function of τ_N^0. Here τ_N^0 denotes the correlation time at which $V_C = 0$.

where A is approximately 375 μsec (Fig. 11b). V_N^0 means here the threshold voltage of noise inducing the instability without a deterministic field and the factor 6.5 V the threshold at a dc field (i.e., $\tau_N^{-1} = 0$). The above empirical equation probably only holds within the region of parameter space explored in the present study.

Another feature worth mentioning is the fact that although the threshold for DSM is monotonically increasing with increasing noise strength, the difference between the onset value for WD and for DSM is monotonically decreasing toward V_N^{***}. The same holds for GP, although for a different threshold value of V_N.

3.2.2. Dynamical Properties. Figure 12 shows the noise dependence of the linear growth time obtained from the experimental results using Eq. (5). τ_L has a maximum value at the noise intensity $Q \sim 5\ \mathrm{V}^2$, which becomes larger with decreasing ε (Fig. 13). Here V_C is determined from $V_C(Q)$ for each $Q \neq 0$, since the threshold is shifted by the application of noise. Here V_{C0} is V_C at $Q = 0$. The ε-dependence of τ_L is changed in the presence of external noise, as shown in Fig. 14 for $Q = 5.1\ \mathrm{V}^2$. Figure 13 shows the linear onset time as a function of Q near threshold (small ε). τ_L tends to diverge at Q close to $5\ \mathrm{V}^2$ with decreasing ε. Such an anomaly typically occurs when the noise amplitude V_N is of the order of 10–20% of

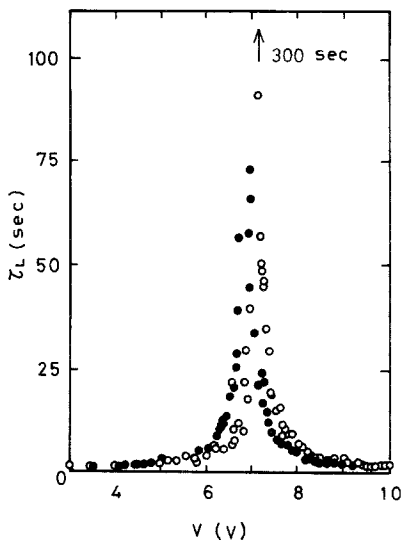

Fig. 12. Typical example of τ_L as a function of the deterministic voltage ($\tau_N = 33$ μsec) for two different noise intensities (sample 4: $d = 100$ μm, $V_{C0} = 6.68$ V). (●) $V_N = 1$ V, (○) $V_N = 2.8$ V.

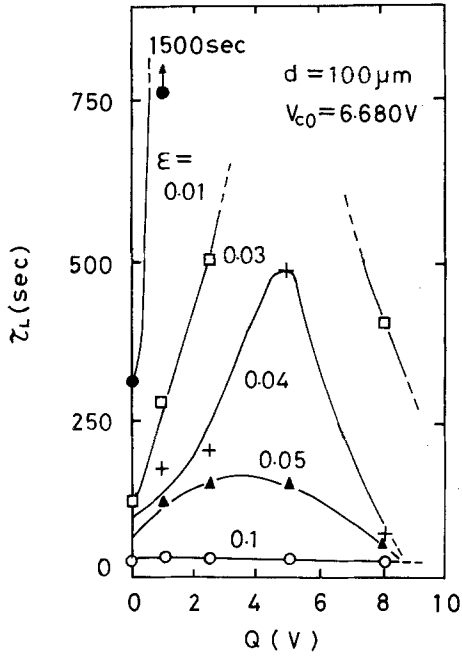

Fig. 13. Growth time τ_L as a function of noise intensity Q (sample 4).

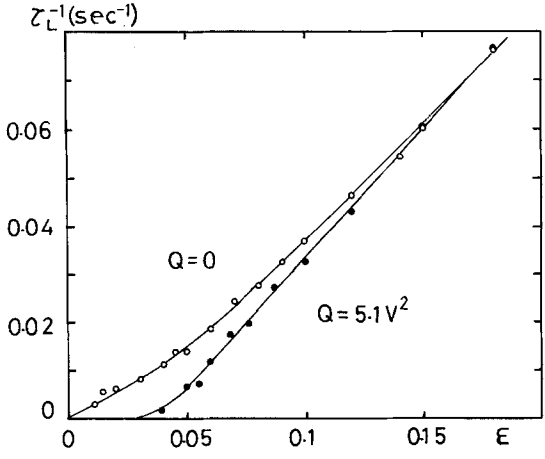

Fig. 14. τ_L as a function of ε (sample 4). (○) $Q=0$, (●) $Q=5.1\ V^2$.

the deterministic amplitude V_C. The linear dependence of τ_L on ε for $Q=0$ is well understood from Eq. (3), but note that for $Q=5.1\ \mathrm{V}^2$ the curve bends to $\tau_L^{-1}=0$, approaching $\varepsilon=0.03$ (Fig. 14). Here $V_C(Q)$ is obtained by the extrapolation of τ_L from large ε. Accordingly, we do not actually observe a pattern at very small ε. We find, however, that the pattern suddenly appears when ε is increased. This might suggest that the transition becomes discontinuous in the presence of noise.[40] Thus, the anomaly at $Q\approx 5\ \mathrm{V}^2$ seems a feature worth noting. In fact, the flow scale λ_X above $Q\approx 5\ \mathrm{V}^2$ seems to change discontinuously from that observed below. In Fig. 15 the wavenumber change of the convective rolls due to the external noise if shown for two different aspect ratios $\Gamma=72$ and 10. This behavior is only observed near threshold (small ε) and at small Q (~ 0.1–$0.2\ V_C^2$) and we therefore infer that the additive noise might play an important role[1,9,22] for this feature. The detailed mechanism for this behavior is unclear.

In the present MSP experiment, ε is always renormalized by $V_C(Q)$ when Q is varied. The initial growth time τ_L becomes much longer very close to $\varepsilon=0$ at $Q>0$ than that at the same value of ε for $Q=0$, i.e., the time the system stays at $\Theta=0$ (the unstable state without noise) becomes longer for $Q_*>Q>0$. Here Q_* is a threshold and of the order of $Q_*^{1/2}\sim 2.5\ \mathrm{V}$. Once the director deformation starts to grow, however, the macroscopic order is built up very quickly. It sometimes seems to be even hysteretic (which would go well with the results presented in ref. 40). This behavior appears to be opposite to that expected from the theory made for a spatially homogeneous system, but with a quadratic noise term. This therefore suggests a different modification of Φ from that predicted

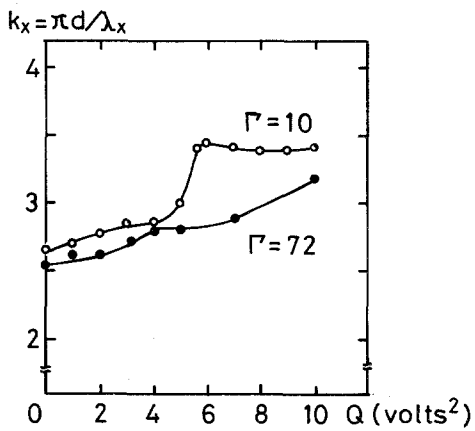

Fig. 15. Wavenumber as a function of Q. (○) aspect ratio $\Gamma=10$, (●) $\Gamma=72$.

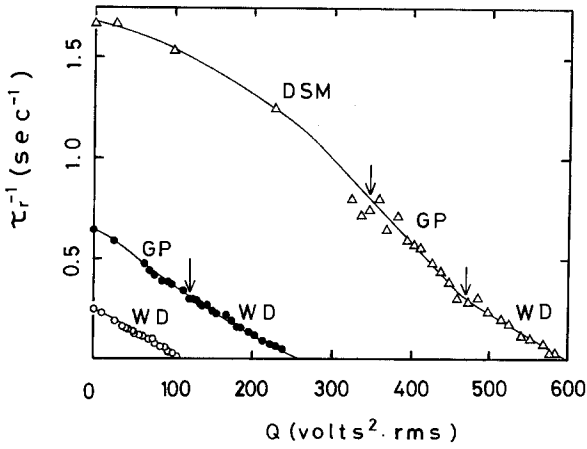

Fig. 16. Nonlinear onset time as a function of noise intensity Q for sample 5: $d = 110\ \mu$m, $V_{C0} = 9.3$ V, aspect ratio 72.

for the Fredericksz transition. Clearly, further investigations are needed theoretically and experimentally on that point.

We also observe that the nonlinear growth time τ_r linearly increases with decreasing Q (Fig. 16). The slope in the GP region is different from that in the WD region, and it is larger for GP. For the spatially homogeneous model

$$\dot{u} = du - b\,|u|^2 u + u\xi \tag{8}$$

such a linear dependence on the noise intensity has been predicted in ref. 1, but obviously the slope changes due to different spatial structures cannot possibly be obtained from Eq. (8). For the DSM state we find a more complicated nonlinear relation between growth time and noise intensity, but again τ_r^{-1} decreases monotonically as a function of noise intensity. As one goes to the turbulent DSM state, an amplitude equation of the type (8) is therefore clearly no longer applicable.

4. SUMMARY AND CONCLUSION

The results obtained from the present study of multiplicative stochastic processes can be summarized as follows.

An externally applied, spatially homogeneous noise with correlation time $\tau_N \ll \tau_C$ can (1) delay the onset of convection, (2) increase the threshold value for the convective onset, and (3) postpone the onset of spatial turbulence.

Furthermore, a different noise dependence of the growth time is observed as the flow structure changes, e.g., from Williams domains to the grid pattern and to the dynamic scattering mode. A most interesting aspect of noise effects is the fact that they can lead to a different structure at the onset of the first instability $[V_C(V_N)]$ with an increase in V_N as shown in Fig. 9. We call this process a structure change induced by external noise. The linear theory by Behn and Mueller[27] can give a destabilization of the instability in EHD. However, we stress that the threshold shift due to noise is not linear and changes its curvature as a function of noise intensity at several noise intensities, which is different from the predictions of the linear theory. We also note that the externally applied noise field destabilizes the convective system at $\tau_N > \tau_N^*$, but stabilizes it for $\tau_N < \tau_N^*$. Successive changes in curvature of the threshold voltage as a function of the noise intensity have been observed and their dependence on the correlation time of the noise has been studied.

ACKNOWLEDGMENTS

This work has been supported by a Grant-in-Aid for Scientific Research (no. 62460037) from the Ministry of Education, Science and Culture of Japan. H.R.B. thanks the Deutsche Forschungsgemeinschaft for support of his work through Sonderforschungsbereich 237-Unordnung und grosse Fluktuationen.

REFERENCES

1. A. Schenzle and H. Brand, *Phys. Rev. A* **20**:1628 (1979).
2. A. Schenzle and H. Brand, *Opt. Commun.* **27**:845 (1978).
3. H. Brand, R. Graham, and A. Schenzle, *Opt. Commun.* **32**:359 (1982).
4. H. Brand and A. Schenzle, *Phys. Lett. A* **81**:321 (1981).
5. K. Kaminishi, R. Roy, R. Short, and L. Mandel, *Phys. Rev. A* **24**:370 (1981).
6. R. Graham, M. Hohnerbach, and A. Schenzle, *Phys. Rev. Lett.* **48**:396 (1982).
7. R. Short, L. Mandel, and R. Roy, *Phys. Rev. Lett.* **49**:647 (1982).
8. A. Schenzle and R. Graham, *Phys. Lett. A* **98**:319 (1983).
9. H. R. Brand, *Prog. Theor. Phys.* **72**:1255 (1984).
10. R. F. Fox, G. E. James, and R. Roy, *Phys. Rev. Lett.* **52**:1778 (1984).
11. R. F. Fox, *Phys. Rev. A* **34**:3405 (1986).
12. S. Zhu, A. W. Yu, and R. Roy, *Phys. Rev. A* **34**:4333 (1986).
13. L. A. Lugiato, A. Colombo, G. Broggi, and R. J. Horowicz, *Phys. Rev. A* **33**:4496 (1986).
14. P. Lett, E. C. Gage, and T. H. Chyba, *Phys. Rev. A* **35**:746 (1987).
15. W. Horsthemke, C. R. Doering, R. Lefever, and A. S. Chi, *Phys. Rev. A* **31**:1123 (1985).
16. M. San Miguel, *Phys. Rev. A* **32**:3811 (1985).
17. F. Sagues and M. San Miguel, *Phys. Rev. A* **32**:1843 (1985).
18. F. Sagues and M. San Miguel, *Phys. Rev. A* **33**:2769 (1986).
19. M. San Miguel and F. Sagues, *Phys. Rev. A* **36**:1883 (1987).

20. S. Kabashima, S. Kogure, T. Kawakubo, and T. Okada, *J. Appl. Phys.* **50**:6296 (1979).
21. J. M. Sancho, M. San Miguel, H. Yamazaki, and T. Kawakubo, *Physica A* **116**:560 (1982).
22. R. Mannella, S. Faetti, P. Grigolini, P. V. E. McClintock, and F. E. Moss, *J. Phys. A* **19**:L699 (1986).
23. S. Kai, T. Kai, M. Takata, and K. Hirakawa, *J. Phys. Soc. Jpn.* **47**:1379 (1979).
24. H. Brand and A. Schenzle, *J. Phys. Soc. Jpn.* **48**:1382 (1980).
25. T. Kawakubo, A. Yanagita, and S. Kabashima, *J. Phys. Soc. Jpn.* **50**:1451 (1981).
26. H. R. Brand, S. Kai, and S. Wakabayashi, *Phys. Rev. Lett.* **54**:555 (1985).
27. U. Behn and R. Mueller, *Phys. Lett. A* **113**:85 (1985); R. Mueller and U. Behn, preprint, Electrohydrodynamic instabilities in nematic liquid crystals under dichotomous parametric modulation (1987).
28. S. Kai, in *Noise in Nonlinear Dynamical Systems*, F. E. Moss and P. V. E. McClintock, eds. (Cambridge University Press, Cambridge, 1988).
29. H. R. Brand, in *Noise in Nonlinear Dynamical Systems*, F. E. Moss and P. V. E. McClintock, eds. (Cambridge University Press, Cambridge, 1988).
30. M. Suzuki, *Adv. Chem. Phys.* **46**:195 (1981).
31. H. Brand, A. Schenzle, and G. Schroder, *Phys. Rev. A* **25**:2324 (1982).
32. F. Moss and G. V. Welland, *Phys. Rev. A* **25**:3389 (1982).
33. R. Graham and A. Schenzle, *Phys. Rev. A* **25**:1731 (1982).
34. J. Smythe, F. Moss, and P. V. E. McClintock, *Phys. Rev. Lett.* **51**:1062 (1983).
35. W. Horsthemke and R. Lefever, *Noise-Induced Transitions* (Springer, New York, 1984).
36. F. Sagues, M. San Miguel, and J. M. Sancho, *Z. Phys. B* **55**:269 (1984).
37. H. R. Brand, *Phys. Rev. Lett.* **54**:600 (1985).
38. F. Pasquale, J. M. Sancho, M. San Miguel, and P. Tartaglia, *Phys. Rev. A* **33**:4360 (1986).
39. R. Graham and A. Schenzle, *Phys. Rev. A* **26**:1676 (1982).
40. M. V. Feigelman and I. E. Staroselsky, *Z. Phys. B* **62**:261 (1986).
41. S. Kai, H. Fukunaga, and H. R. Brand, *J. Phys. Soc. Jpn.* **56**:3759 (1987).
42. P. G. de Gennes, *The Physics of Liquid Crystals*, 3rd ed. (Clarendon Press, Oxford, 1982).
43. S. Kai, K. Yamaguchi, and K. Hirakawa, *Jpn. J. Appl. Phys.* **14**:1653 (1975).
44. K. Hirakawa and S. Kai, *Mol. Cryst. Liq. Cryst.* **40**:261 (1977).
45. S. Kai and K. Hirakawa, *Prog. Theor. Phys. Suppl.* **64**:212 (1978).
46. S. Kai, S. Wakabayashi, and M. Imasaki, *Phys. Rev. A* **33**:2612 (1986).
47. P. Pieranski, F. Brochard, and E. Guyon, *J. Phys.* (Paris) **34**:35 (1973).
48. W. Zimmermann and L. Kramer, *Phys. Rev. Lett.* **55**:402 (1985); L. Kramer, W. Zimmermann, E. Bodenschatz, and W. Pesch, in *Propagative Processes far from Equilibrium*, J. E. Wesfreid *et al.*, eds. (Springer, New York, 1988); private communication.
49. A. Joets and R. Ribotta, *J. Phys.* (Paris) **47**:595, 739 (1986).